Periodic Variability in the Large-Scale Southern Hemisphere Atmospheric Circulation

David W. J. Thompson and Elizabeth A. Barnes

Science **343**, 641 (2014);
DOI: 10.1126/science.1247660

Periodic Variability in the Large-Scale Southern Hemisphere Atmospheric Circulation

David W. J. Thompson* and Elizabeth A. Barnes

Periodic behavior in the climate system has important implications not only for weather prediction but also for understanding and interpreting the physical processes that drive climate variability. Here we demonstrate that the large-scale Southern Hemisphere atmospheric circulation exhibits marked periodicity on time scales of approximately 20 to 30 days. The periodicity is tied to the Southern Hemisphere baroclinic annular mode and emerges in hemispheric-scale averages of the eddy fluxes of heat, the eddy kinetic energy, and precipitation. Observational and theoretical analyses suggest that the oscillation results from feedbacks between the extratropical baroclinicity, the wave fluxes of heat, and radiative damping. The oscillation plays a potentially profound role in driving large-scale climate variability throughout much of the mid-latitude Southern Hemisphere.

The most robust periodic variability in the climate system is found in association with orbital forcing (*1*). The rotation of Earth on its axis drives the diurnal cycle; the axial tilt of Earth, combined with its orbit about the Sun, causes the seasonal cycle; and low-frequency variations in the eccentricity, axial tilt, and precession of Earth's orbit together produce periodic climate variability on time scales of millennia. Periodic heating from the Sun creates atmospheric thermal tides on a range of time scales.

Large-scale atmospheric variability due to internal climate dynamics is generally not periodic. The most notable exceptions are found in the tropics. The Madden-Julian oscillation is characterized by circulation and precipitation anomalies that propagate eastward in the tropical troposphere on time scales of ~40 to 70 days (*2*). The quasi-biennial oscillation is marked by alternating eastward and westward wind anomalies that propagate downward in the tropical stratosphere on time scales of ~24 to 27 months (*3*). The El Niño/Southern Oscillation phenomenon is weakly periodic, with enhanced spectral power on periods of ~2 to 7 years (*4*). In contrast, large-scale atmospheric variability in the extratropics is typically not periodic but rather is consistent with Gaussian red noise (*5*, *6*).

Recent evidence suggests an additional source of periodic variability in the climate system that has been largely overlooked in previous work. The periodicity emerges in the extratropical Southern Hemisphere and is associated with variability in the Southern Hemisphere baroclinic annular mode [BAM (*7*)]. Here we illustrate the robustness and climate implications of quasiperiodic behavior in the BAM, explore the dynamical mechanisms that give rise to it, and demonstrate the robustness of similar periodic behavior in a hierarchy of numerical models.

Department of Atmospheric Science, Colorado State University, Fort Collins, CO, USA.

*Corresponding author. E-mail: davet@atmos.colostate.edu

The Southern Hemisphere BAM is the baroclinic analog of the more widely studied southern annular mode (SAM). The two structures play very different roles in cycling energy through the Southern Hemisphere circulation. The SAM dominates the variance in the Southern Hemisphere zonal-mean kinetic energy, whereas the BAM dominates the variance in the Southern Hemisphere eddy kinetic energy (*8*). The SAM is driven by the variations in eddy fluxes of momentum (*6*), whereas the BAM is driven by variations in the eddy fluxes of heat (*7*). The SAM is marked by north-south vacillations in the extratropical jet about its climatological axis (*9*, *10*), whereas the BAM is marked by pulsing of the extratropical eddy kinetic energy throughout much of the middle to high-latitude Southern Hemisphere (*7*). Finally, the SAM is well modeled as Gaussian red noise (*9*), whereas the BAM exhibits marked periodicity on time scales of ~20 to 30 days (*7*).

The BAM is characterized by fluctuations in the lower tropospheric eddy fluxes of heat and upper tropospheric eddy kinetic energy that span much of the Southern Hemisphere (Fig. 1, A and C) (*7, 11, 12, 13*). It is thus associated with variations in both the generation and amplitude of wave activity throughout much the Southern Hemisphere (*14*). The BAM also has a distinct signature in precipitation: Periods of enhanced eddy kinetic energy (the positive polarity of the BAM) are marked by increases in precipitation throughout much of the Southern Hemisphere midlatitudes (Fig. 1E) (*15*). The linkages between the BAM and the hemispheric means of all three key physical fields are highly robust (Table 1). Consistent with the life cycle of developing baroclinic waves (*16*), the signatures of the BAM in the eddy fluxes of heat and precipitation precede the signature of the BAM in upper tropospheric eddy kinetic energy by ~1 day [see also (*7*)].

The periodicity in the BAM extends to the hemispheric-mean time series of wave amplitudes in the upper troposphere (Fig. 1B), wave generation in the lower troposphere (Fig. 1D) (*14*), and precipitation (Fig. 1F) (*17*). The spectral peaks in all three time series are based on a large number of degrees of freedom and are extremely robust (*17*). The periodicity in the large-scale Southern Hemisphere circulation is also reproducible in hemispheric-mean remotely sensed precipitation derived from the Advanced Microwave Scanning Radiometer (AMSR)-E instrument [Fig. 1F, red line (*11*)] and is thus not an artifact of the ERA-Interim reanalysis (*11*). A similar spectral peak was noted in eddy kinetic energy derived from only 1 year of relatively sparse balloon measurements taken in 1971–1972 for the Eole experiment (*18*) and in only one winter of zonal-wind measurements taken in 1979 for the Global Weather Experiment (*19*). The spectra in Fig. 1 reveal that Southern Hemisphere–mean atmospheric wave activity and precipitation exhibit robust periodicity on ~20 to 30 time scales in more than 30 years of data.

What physical process gives rise to the observed periodic behavior in Southern Hemisphere extratropical circulation? The periodicity in the hemispheric-mean fields of eddy kinetic energy and the eddy fluxes of heat indicates a negative feedback in the dynamics that drive their variability. Such a feedback is known to exist between the extratropical baroclinicity and the wave fluxes of heat. Baroclinic instability theory predicts that periods of enhanced baroclinicity lead to rapid growth in baroclinic waves and thus to periods of anomalously poleward eddy heat fluxes (*20*, *21*). Conversely, the thermodynamic energy equation dictates that anomalously poleward eddy heat fluxes lead to reductions in the baroclinicity [through the convergence and divergence of the eddy heat flux (*20*)]. The baroclinicity is known to play a key role in setting the climatological-mean structure of the wave fluxes of heat in both hemispheres (*22, 23, 24*). Two-way feedbacks between variability in the baroclinicity and the growth of baroclinic waves are observed in the Northern Hemisphere (*25*). The observational analyses shown in Fig. 2 confirm that analogous feedbacks are also observed in the Southern Hemisphere.

Figure 2 shows the eddy fluxes of heat (contours) and the baroclinicity (shading) regressed on standardized values of Southern Hemisphere–mean eddy heat fluxes as a function of lag and latitude (Fig. 2A) and lag and height (Fig. 2B). The Southern Hemisphere mean is defined as the area and density weighted average calculated over 30° to 70°S and 250 to 950 hPa. The heat flux index is multiplied by –1, so that positive values of the index denote poleward (southward) heat fluxes and vice versa. The baroclinicity is expressed in terms of the Eady growth rate, which provides a quantitative estimate of the growth rate of baroclinic eddies

$$\sigma_{BI} = 0.31 g N^{-1} T^{-1} \left| \frac{\partial T}{\partial y} \right| \qquad (1)$$

where σ_{BI} is the growth rate, g is the acceleration due to gravity, N is the Brunt-Väisälä frequency, T is temperature, and y is the meridional direction (*26*).

By construction, the regression map in Fig. 2A is dominated by large poleward heat fluxes (solid contours) that peak around lag 0. The poleward heat fluxes persist for several days (Fig. 2A) and extend throughout the Southern Hemisphere troposphere (Fig. 2B). The period immediately after the peak in the poleward eddy fluxes of heat is marked by a rapid reduction in the baroclinicity (blue shading at positive lag), as expected from the thermodynamic energy equation. The period immediately preceding the peak in the poleward eddy fluxes is marked by positive anomalies in the baroclinicity (warm colors at negative lag), which is consistent with baroclinic instability theory. The precursor in the baroclinicity at negative lag has a slightly longer time scale than the response at positive lag. In both cases, the anomalies in the baroclinicity extend throughout the depth of the troposphere and peak just above the 500-hPa level (Fig. 2B).

The observational results presented in Fig. 2 suggest that the BAM is associated with two-way feedbacks between the baroclinicity and eddy fluxes of heat. The periodicity driven by such feedbacks can be explored in a simple stochastic model based on linearized versions of Eq. 1 and the thermodynamic energy equation.

To develop the model, we first applied two simplifying assumptions to Eq. 1 to generate a prognostic equation for the anomalous eddy fluxes of heat averaged over the Southern Hemisphere baroclinic zone. We assumed that (i) the growth rate of baroclinic waves (the left-hand side of Eq. 1) is proportional to the time rate of change of the eddy flux of heat, and (ii) variations in the baroclinicity (the right-hand side of Eq. 1) are due primarily to variability in the meridional temperature gradient. The former assumption follows from the direct relationship between the vertical flux of wave activity and the eddy flux of heat (*27*). The latter assumption is supported by the fact that the changes in the Eady growth rate shown in Fig. 2 are dominated by the variations in the meridional temperature gradient (supplementary materials). Equation 1 was then linearized about the climatological mean state to yield an expression for the time rate of change of the eddy fluxes of heat as a function of the baroclinicity

$$\frac{\partial}{\partial t}\langle v^* T^* \rangle = -\alpha \langle b \rangle + \varepsilon(t) \qquad (2)$$

where v^*T^* and $b \overset{\text{def}}{=} \frac{\partial T}{\partial y}$ denote the anomalous eddy fluxes of heat and meridional temperature gradient, respectively, and the brackets denote the average over the Southern Hemisphere baroclinic zone (defined here as 40° to 55°S). The regression coefficient α corresponds to the amplitude of the feedback between the baroclinicity and the eddy fluxes of heat. The term $\varepsilon(t)$ reflects stochastic forcing of the heat fluxes by weather "noise" and prevents the model from reaching a steady state where $\langle v^* T^* \rangle = \langle b \rangle = 0$.

We then applied two simplifying assumptions to the zonal-mean thermodynamic energy equation to form a prognostic equation for the anomalous baroclinicity. In this case, we assumed that (i) the net forcing of the baroclinicity by the wave fluxes of heat is linearly proportional to the heat fluxes themselves, and (ii) the damping of the baroclinicity due to both adiabatic and diabatic processes can be modeled as Newtonian cooling. The resulting equation was subsequently linearized about the climatological mean state to yield an expression for the time rate of change of the baroclinicity as a function of the heat fluxes

$$\frac{\partial \langle b \rangle}{\partial t} = \beta \langle v^* T^* \rangle - \frac{\langle b \rangle}{\tau} \qquad (3)$$

where the regression coefficient β corresponds to the amplitude of the feedback between the eddy fluxes

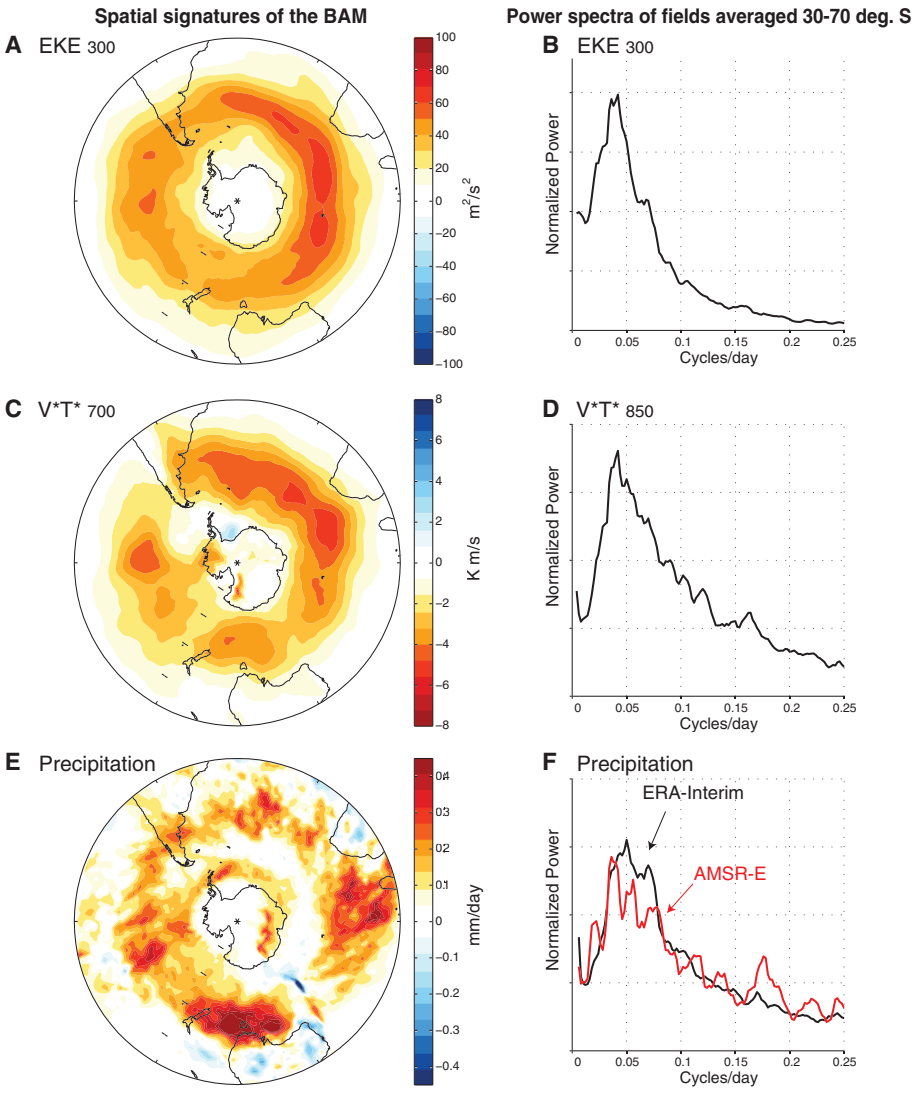

Fig. 1. (A to F) Space and time signatures of the Southern Hemisphere BAM. The left panels show the fields indicated regressed onto the BAM index time series (*12, 13, 15*). The right panels show power spectra for hemispheric averages of the fields indicated (*17*). Red values in (C) denote southward (negative) heat fluxes. The spectra in (F) show results for precipitation derived from ERA-Interim [black (*11*)] and AMSR-E [red (*11*)]. All other panels are based on the ERA-Interim model (*11*). As discussed in the text, the heat fluxes and precipitation peak 1 day before the peak in eddy-kinetic energy, and thus the regressions in (C) and (E) are lagged by –1 day with respect to the BAM index.

Table 1. Correlations between the BAM index (*12*) and hemispheric means (30° to 70°S) of the fields indicated. Correlations are based on all days of 1979–2010 (11,678 days). The BAM is defined as the leading PC of eddy-kinetic energy (*12*). As discussed in the text, the heat fluxes and precipitation peak 1 day before the peak in eddy-kinetic energy. All correlations are statistically different from zero at the 99% level, based on a one-tailed test of the *t* statistic. EKE is the eddy kinetic energy.

Field	$[v^*T^*]$ at 850 hPa	EKE at 300 hPa	Total precipitation
Correlation with BAM index	$r = -0.67$ (lag –1)	$r = +0.98$ (lag 0)	$r = -0.49$ (lag –1)

of heat and the baroclinicity. The Newtonian cooling term $\frac{\langle b \rangle}{\tau}$ reflects the damping of the baroclinicity by both diabatic processes and vertical motion. The parameter τ denotes the damping time scale.

Equations 2 and 3 were then solved numerically and analytically to generate expressions for the model eddy fluxes of heat and their periodicity. Figure 3A shows the frequency of oscillation in $\langle v^* T^* \rangle$ from the analytic solution (neglecting the stochastic term; see the supplementary materials) as a function of the feedback parameters (abscissa) and damping time scale (ordinate). Figure 3B shows the spectra of $\langle v^* T^* \rangle$ from the numerical solution with the stochastic term, using the feedbacks observed at the 500-hPa level. The solutions to the model and the calculation of the observed parameters are discussed in the supplementary materials.

The simple coupled model yields several key insights into the conditions that lead to oscillatory behavior in the Southern Hemisphere circulation.

1) As shown in the supplementary materials, the model heat fluxes oscillate at a frequency given by

$$\omega = \frac{24 \times 3600}{2\pi} Im\left\{\left(\sqrt{\frac{1}{(2\tau)^2} - \alpha\beta}\right)\right\} \text{day}^{-1} \quad (4)$$

The frequency of the oscillation in $\langle v^* T^* \rangle$ is thus a function of the product of the feedback parameters $\alpha\beta$ and the damping time scale τ (Eq. 4). The frequency of the oscillation increases as the feedback amplitudes increase and/or as the damping time scale increases.

2) The derivation of the model parameters from observations is described in the supplementary materials. The red circles in Fig. 3A indicate the frequencies predicted by the model based on the observed feedbacks and damping time scales calculated at all tropospheric levels from 950 to 300 hPa. The range of predicted oscillation frequencies is slightly lower than the observed range, depending on the level chosen to calculate the observed feedbacks. When the observed middle tropospheric feedbacks are inserted into Eq. 4, the model heat fluxes oscillate at a frequency that is strikingly similar to the observed frequency (red curve in Fig. 3B).

3) Oscillating solutions in $\langle v^* T^* \rangle$ are only possible when the damping time scale $\tau > \frac{1}{2\sqrt{\alpha\beta}}$. For the observed middle tropospheric values of α and β, the model heat fluxes only oscillate if the damping time scale is longer than ~2 days (Fig. 3A). When the damping time scale is shorter than this value, the spectrum of the model heat fluxes is red (Fig. 3B). From a physical perspective, if the damping is very large (τ is very small), the perturbations in the baroclinicity are damped before they have time to affect the eddy fluxes of heat.

The results of the simple model given in Eqs. 2 and 3 suggest that periodicity in the extratropical wave fluxes of heat (and thus the eddy kinetic energy) should arise in any numerical model that includes two-way interactions between the baroclinicity and baroclinic waves. Figure 4 shows the spectra of the hemispheric-mean eddy fluxes of heat and eddy kinetic energy from three general circulation models (GCMs) of varying complexity (*28*): (i) a fully coupled atmosphere/ocean GCM (top row); (ii) an aquaplanet GCM with no orography, simplified radiation, and a slab ocean (middle row); and (iii) a dry dynamical core with parameterized physics (bottom row). All three classes of models exhibit periodic behavior in the hemispheric-mean eddy heat fluxes and eddy kinetic energy. The similarities between the

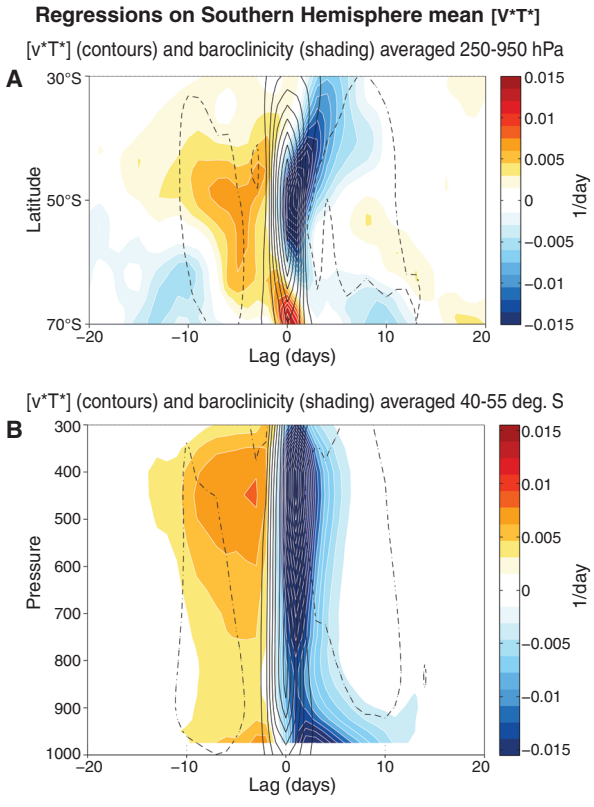

Fig. 2. Regressions on the Southern Hemisphere–mean eddy fluxes of heat. The Southern Hemisphere mean is defined as an average over 30° to 70°S and 250 to 950 hPa. The baroclinicity is quantified as the Eady growth rate (see text). The contour intervals are 0.5 K m/s (**A**) and 0.6 K m/s (**B**). The solid contours denote southward (negative) heat fluxes.

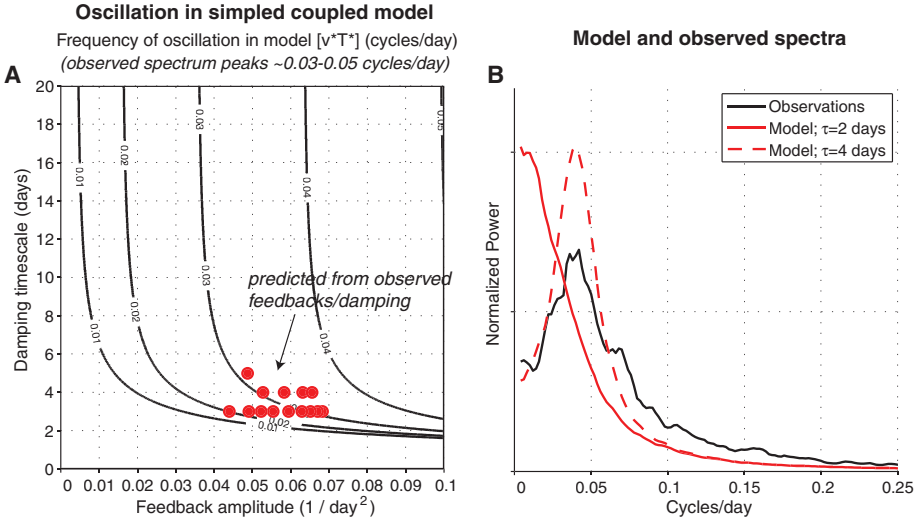

Fig. 3. Simulating periodic behavior in the heat fluxes in a simple coupled model. (A) The analytic solution of the oscillation frequency in the eddy fluxes of heat obtained from the simple model of Eqs. 2 and 3. Results are shown as a function of the product of the model feedback parameters ($\alpha \times \beta$; abscissa) and damping times cale (ordinate). Frequency units are cycles per day. Red circles indicate the range of frequencies predicted from the observed feedbacks and damping time scales at all tropospheric levels. **(B)** Power spectra derived from the simple model using the feedback parameters at 500 hPa for the damping time scales indicated. The observed spectrum is for Southern Hemisphere mean eddy kinetic energy and is reproduced from Fig. 1B. See the supplementary materials for details of the calculations.

modeled and observed spectra are most pronounced in the case of the fully coupled and aquaplanet GCMs. The dry dynamical core also exhibits broad spectral power on weekly time scales in the eddy kinetic energy and eddy fluxes of heat, but the peak in the spectrum of the eddy heat fluxes extends to higher frequencies than it does in the observations.

The observed periodicity in the Southern Hemisphere circulation is reminiscent of that proposed more than 60 years ago in association with the Northern Hemisphere "index cycle" (*29*, *30*). Research on the index cycle waned in the 1960s because of a lack of supporting observational evidence (*31*). We were likewise unable to find evidence of oscillatory behavior in the Northern Hemisphere that was similar to that shown here. The apparent lack of analogous periodicity in the large-scale Northern Hemisphere circulation may be due to the relatively narrow west-east scale of the Northern Hemisphere storm tracks. It may also be due to the relatively large climatological-mean baroclinicity found over the western North Atlantic and North Pacific basins due to the land-sea contrasts there. Both factors could limit the ability of baroclinicity anomalies associated with atmospheric variability to influence the heat fluxes: the former because anomalies in baroclinicity may be advected downstream of the storm tracks before they influence the heat fluxes; the latter because the anomalies in baroclinicity due to atmospheric variability are much smaller than those due to the Northern Hemisphere climatological-mean state.

The results shown here demonstrate that the large-scale Southern Hemisphere circulation exhibits robust periodicity in a range of key physical parameters. They reveal that the periodicity is consistent with two-way feedbacks between the baroclinicity and the eddy fluxes of heat. They also reveal that similar periodicity is evident in a hierarchy of numerical models. To what extent the periodicity in the baroclinic annular mode contributes to the variance in local weather over specific regions of the Southern Hemisphere remains to be determined. But the periodicity clearly has potentially profound implications for understanding and predicting Southern Hemisphere climate variability over broad spatial scales.

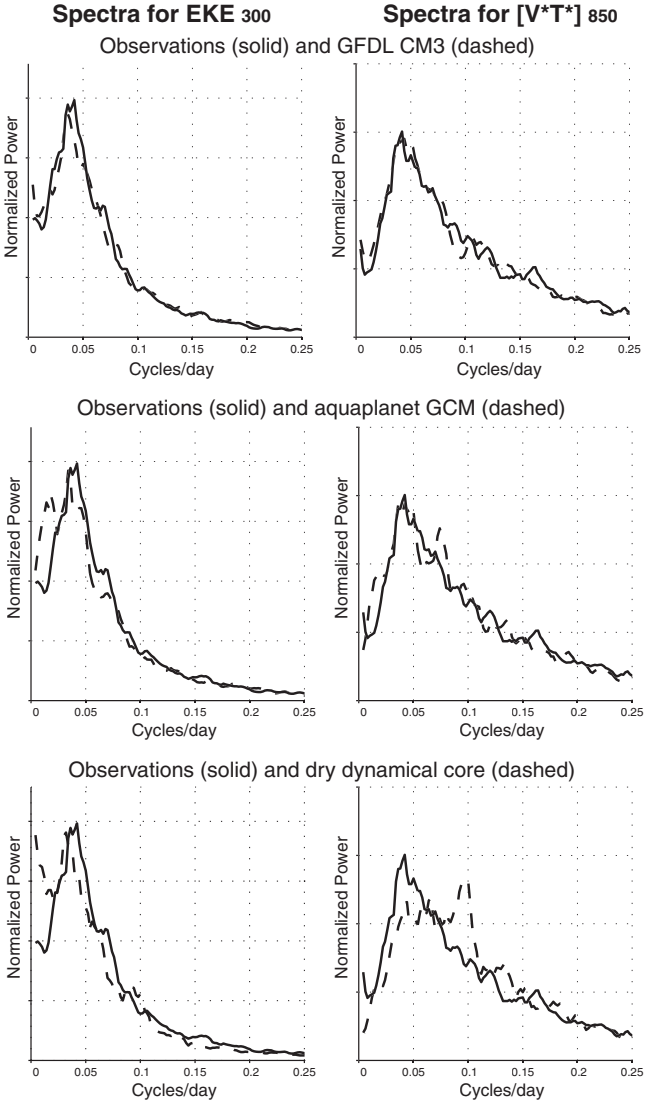

Fig. 4. Comparing observed and simulated power spectra. (Left) Spectra of eddy kinetic energy at 300 hPa averaged 30° to 70°S. **(Right)** Spectra of the eddy fluxes of heat at 850 hPa averaged 30° to 70°S. Solid lines show the observed spectra; dashed lines show spectra for the climate models indicated on the figure. Models are described in (*28*). The calculation of the spectra is described in (*17*).

References and Notes

1. D. L. Hartmann, *Global Physical Climatology* (Academic Press, San Diego, CA, 1994).
2. C. Zhang, *Rev. Geophys.* **43**, RG2003 (2005).
3. M. P. Baldwin *et al*., *Rev. Geophys.* **39**, 179–229 (2001).
4. E. M. Rasmusson, T. H. Carpenter, *Mon. Weather Rev.* **110**, 354–384 (1982).
5. S. B. Feldstein, *J. Clim.* **13**, 4430–4440 (2000).
6. D. J. Lorenz, D. L. Hartmann, *J. Atmos. Sci.* **58**, 3312–3327 (2001).
7. D. W. J. Thompson, J. D. Woodworth, *J. Atmos. Sci.*; available online at http://journals.ametsoc.org/loi/atsc (2014).
8. The SAM and southern BAM are defined as the leading empirical orthogonal functions (EOF)/principal components (PC) time series of the zonal-mean kinetic and eddy kinetic energies, respectively. If **X** is a two-dimensional data matrix that samples space and time, then the leading EOF of **X** is the spatial function that explains the largest possible fraction of the variance in **X**. The leading PC of **X** is the expansion coefficient time series associated with the leading EOF. The leading EOF is found as the eigenvector associated with the largest eigenvalue of the covariance matrix of **X**.
9. D. L. Hartmann, F. Lo, *J. Atmos. Sci.* **55**, 1303–1315 (1998).
10. D. W. J. Thompson, J. M. Wallace, *J. Clim.* **13**, 1000–1016 (2000).
11. All observational results except the red curve in Fig. 1F are based on the interim European Centre for Medium-Range Weather Forecasts (ECMWF) Re-Analysis (ERA-Interim) data from 1 January 1979 to 31 December 2010. The red curve in Fig. 1F is based on Version 7 of the Advanced Microwave Scanning Radiometer (AMSR)-E precipitation data, obtained from Remote Sensing Systems. For details of ERA-Interim, see (*32*).
12. The results in the left panel of Fig. 1 and in Table 1 are based on standardized values of the BAM index, defined here as the leading PC of zonal-mean eddy kinetic energy computed over all levels and latitudes within the domain from 1000 to 200 hPa and 20° to 70°S. The data are weighted by the area represented by each grid box and the mass represented by each vertical level in the ERA-Interim before calculating the PC time series.
13. The zonal-mean eddy fluxes of heat and eddy kinetic energy are defined as $[v^*T^*]$ and $\frac{1}{2}[v^{*2} + u^{*2}]$, respectively, where asterisks denote departures from the zonal mean and brackets denote the zonal mean. Eddy fluxes and eddy kinetic energy are calculated from 4*x* daily data before computing daily averages.
14. The eddy fluxes of heat are proportional to the vertical flux of wave activity. Thus, the vertical divergence of the eddy fluxes of heat in the lower troposphere is proportional to the generation of wave activity there.
15. The ERA-Interim precipitation is based on the 12-hour forecast of 12 Greenwich mean time total precipitation. The ERA-Interim precipitation is a model-derived quantity but is calculated using physically consistent parameterizations that link atmospheric motions to precipitation.
16. A. J. Simmons, B. J. Hoskins, *J. Atmos. Sci.* **35**, 414–432 (1978).
17. All spectra are found by (i) Calculating the spectra for subsets of the time series that are 500 days in length. A Hanning window is applied to each subset, and the overlap between adjacent subsets is 250 days. (ii) Averaging the power spectra over all subsets and then applying a three-point running mean to the resulting mean power spectra. Every 10 years of data yield ~40 degrees of freedom per spectral estimate. The spectral estimates in Fig. 1, B, D, and F (black curve) have ~120 degrees of freedom; the spectral estimates

for AMSR-E precipitation shown in Fig. 1F (red curve) have ~40 degrees of freedom.
18. P. J. Webster, J. L. Keller, *J. Atmos. Sci.* **32**, 1283–1301 (1975).
19. J. W. Kidson, *Mon. Weather Rev.* **114**, 1654–1663 (1986).
20. G. K. Vallis, *Atmospheric and Oceanic Fluid Dynamics* (Cambridge Univ. Press, Cambridge, 2006).
21. R. S. Lindzen, B. F. Farrell, *J. Atmos. Sci.* **37**, 1648–1654 (1980).
22. B. J. Hoskins, P. J. Valdes, *J. Atmos. Sci.* **47**, 1854–1864 (1990).
23. P. J. Kushner, I. M. Held, *Geophys. Res. Lett.* **25**, 4213–4216 (1998).
24. H. Nakamura, A. Shimpo, *J. Clim.* **17**, 1828–1844 (2004).
25. D. W. J. Thompson, T. Birner, *J. Atmos. Sci.* **69**, 1811–1823 (2012).
26. The baroclinicity is defined as the meridional slope of the isentropic surfaces relative to Earth's surface. It thus includes two components: the meridional gradient in temperature and the vertical gradient in temperature (i.e., the static stability).
27. D. G. Andrews, M. E. McIntyre, *J. Atmos. Sci.* **33**, 2031–2048 (1976).
28. The Geophysical Fluid Dynamics Laboratory (GFDL) CM3 is a coupled chemistry climate model. The analyses shown here are based on a simulation performed for the Coupled Model Intercomparison Project (CMIP5), phase 5. See (*33*). We analyzed one ensemble of the historical simulation over years 1970–2004. The aquaplanet simulation is identical to that used in (*34*). The model is integrated at T85 resolution for 21 years, with the first 2 years discarded for spin-up. All model parameters are set to the values from the control experiment of Frierson *et al*. (*34*). The idealized dry GCM is the GFDL spectral dry dynamical core of (*35*). The model does not include radiation or moisture and uses Newtonian relaxation to a zonally symmetric equilibrium temperature profile and Rayleigh damping of the low-level winds to simulate boundary layer friction. The model is integrated at T42 (42-wave triangular truncation) resolution for 6000 days with 2000 days for spin-up. Both the aquaplanet and the dry dynamical core do not have topography and are run under perpetual equinoctial conditions with no diurnal cycle.
29. C.-G. Rossby, H. C. Willett, *Science* **108**, 643–652 (1948).
30. J. Namias, *J. Meteorol.* **7**, 130–139 (1950).
31. J. M. Wallace, H.-H. Hsu, *Tellus* **37A**, 478–486 (1985).
32. D. P. Dee *et al*., *Q. J. R. Meteorol. Soc.* **137**, 553–597 (2011).
33. L. J. Donner *et al*., *J. Clim.* **24**, 3484–3519 (2011).
34. D. M. W. Frierson, I. M. Held, P. Zurita-Gotor, *J. Atmos. Sci.* **63**, 2548–2566 (2006).
35. I. M. Held, M. J. Suarez, *Bull. Am. Meteorol. Soc.* **75**, 1825–1830 (1994).

Acknowledgments: We thank R. Garreaud and J. M. Wallace for helpful discussion of the results, R. Barnes for insight into the analytic model, S. Wills for assistance with the AMSR-E data, and three anonymous reviewers for helpful comments on the manuscript. D.W.J.T. is supported by the NSF Climate Dynamics program.

Supplementary Materials

www.sciencemag.org/content/343/6171/641/suppl/DC1
Supplementary Text
Figs. S1 and S2
Reference

25 October 2013; accepted 7 January 2014
10.1126/science.1247660

A Promiscuous Intermediate Underlies the Evolution of LEAFY DNA Binding Specificity

Camille Sayou,[1,2,3,4]* Marie Monniaux,[1,2,3,4]* Max H. Nanao,[5,6]*† Edwige Moyroud,[1,2,3,4]*‡ Samuel F. Brockington,[7] Emmanuel Thévenon,[1,2,3,4] Hicham Chahtane,[1,2,3,4] Norman Warthmann,[8]§ Michael Melkonian,[9] Yong Zhang,[10] Gane Ka-Shu Wong,[10,11] Detlef Weigel,[8] François Parcy,[1,2,3,4,12]† Renaud Dumas[1,2,3,4]

Transcription factors (TFs) are key players in evolution. Changes affecting their function can yield novel life forms but may also have deleterious effects. Consequently, gene duplication events that release one gene copy from selective pressure are thought to be the common mechanism by which TFs acquire new activities. Here, we show that LEAFY, a major regulator of flower development and cell division in land plants, underwent changes to its DNA binding specificity, even though plant genomes generally contain a single copy of the *LEAFY* gene. We examined how these changes occurred at the structural level and identify an intermediate LEAFY form in hornworts that appears to adopt all different specificities. This promiscuous intermediate could have smoothed the evolutionary transitions, thereby allowing LEAFY to evolve new binding specificities while remaining a single-copy gene.

The rewiring of transcriptional networks is an important source of evolutionary novelty (*1*–*3*). Variation often occurs through changes in cis-regulatory elements, which are DNA sequences that contain binding sites for transcription factors (TFs) regulating nearby genes (*3*, *4*). There is less evidence for regulatory changes affecting the protein-coding sequence of TFs. Such changes are expected to be under highly stringent selection because they could impair the expression of many downstream targets. Gene duplication provides a solution to this dilemma, as additional TF gene copies may acquire new functions, provided that the aggregate copies fulfill the function of the original TF (*5*). Indeed, TF DNA binding specificity has been shown to diversify within multigene families (*6*, *7*). In some cases, however, TF coding genes remain as single-copy genes because of phenomena such as paralog interference (*8*), which can impede neofunctionalization. When essential TFs are maintained as single-copy genes, the extent to which they can evolve is not clear. To address this question, we examined the *LEAFY (LFY)* gene as an evolutionary model.

Except in gymnosperms, in which two paralogs (*LEAFY* and *NEEDLY*) are usually present (Fig. 1A), *LFY* exists mostly as a single-copy gene in land plants (*9*). *LFY* plays essential roles as a key regulator of floral identity in angiosperms, as well as in cell division in the moss *Physcomitrella patens* (*10*). *LFY* encodes a TF that binds DNA through a highly conserved dimeric DNA binding domain (DBD) (*11*). Despite this conservation, PpLFY1, a LFY homolog from the moss *P. patens*, is unable to bind the DNA sequence recognized by LFY from *Arabidopsis thaliana* (AtLFY) (*9*), suggesting that LFY DNA binding specificity might have changed during land plant evolution.

We mined the transcriptomes from algal species, whose origin predates the divergence of mosses and tracheophytes, and found *LFY* homologs in six species of streptophyte green algae (Fig. 1A and fig. S1) (see also supplementary materials and methods). Thus, *LFY* is not specific to land plants. Despite this extended ancestry, the LFY-DBD sequence, including the amino acids in direct contact with DNA, remains highly conserved (Fig. 1B and fig. S1). We used high-throughput SELEX (systematic evolution of ligands by exponential enrichment) (*12*) experiments to systematically analyze the DNA binding specificity of LFY proteins from each group of plants. After

[1]CNRS, Laboratoire de Physiologie Cellulaire et Végétale (LPCV), UMR 5168, 38054 Grenoble, France. [2]Université Grenoble Alpes, LPCV, F-38054 Grenoble, France. [3]Commissariat à l'Energie Atomique et aux Energies Alternatives, Direction des Sciences du Vivant, Institut de Recherches en Technologies et Sciences pour le Vivant, LPCV, F-38054 Grenoble, France. [4]Institut National de la Recherche Agronomique, LPCV, F-38054 Grenoble, France. [5]European Molecular Biology Laboratory (EMBL), 6 Rue Jules Horowitz, BP 181, 38042 Grenoble, France. [6]Unit of Virus Host-Cell Interactions, Université Grenoble Alpes–EMBL–CNRS, UMI 3265, 6 Rue Jules Horowitz, 38042 Grenoble Cedex 9, France. [7]Department of Plant Sciences, University of Cambridge, Downing Street, Cambridge CB2 3EA, UK. [8]Department of Molecular Biology, Max Planck Institute for Developmental Biology, 72076 Tübingen, Germany. [9]Botanisches Institut, Lehrstuhl I, Universität zu Köln, Biozentrum Köln, Zülpicher Strasse 47b, 50674 Köln, Germany. [10]Beijing Genomics Institute (BGI)–Shenzhen, Beishan Industrial Zone, Yantian District, Shenzhen 518083, China. [11]Department of Biological Sciences, Department of Medicine, University of Alberta, Edmonton, Alberta T6G 2E9, Canada. [12]Centre for Molecular Medicine and Therapeutics, Child and Family Research Institute, University of British Columbia, Vancouver, British Columbia V5Z 4H4, Canada.

*These authors contributed equally to this work.
†Corresponding author. E-mail: francois.parcy@cea.fr (F.P); mnanao@embl.fr (M.H.N.)
‡Present address: Department of Plant Sciences, University of Cambridge, Downing Street, Cambridge CB2 3EA, UK.
§Present address: Research School of Biology, The Australian National University, Acton, ACT 0200, Australia.